



Repositorio Institucional de la Universidad Autónoma de Madrid

<https://repositorio.uam.es>

Esta es la **versión de autor** del artículo publicado en:
This is an **author produced version** of a paper published:

ChemPhotoChem 2 (2018): 1-13

DOI: <https://doi.org/10.1002/cptc.201800169>

Copyright: © 2018 Wiley-VCH Verlag GmbH & Co. KGaA,
Weinheim

El acceso a la versión del editor puede requerir la suscripción del recurso
Access to the published version may require subscription

The role of electronic triplets and high-lying singlet states in the deactivation mechanism of the parent BODIPY: an ADC(2) and CASPT2 study.

Martina De Vetta,^{a,b} Leticia González^a, and Inés Corral^{b,c}*

a. Institute of Theoretical Chemistry, Faculty of Chemistry, University of Vienna, Währinger Str. 17, A-1090 Wien, Austria

b. Departamento de Química, Universidad Autónoma de Madrid, C/ Francisco Tomás y Valiente 7, 28049 Cantoblanco, Madrid, Spain

c. IADCHEM. Institute for Advanced Research in Chemistry, Universidad Autónoma de Madrid, C/ Francisco Tomás y Valiente 7, 28049 Cantoblanco, Madrid, Spain

Corresponding Author:

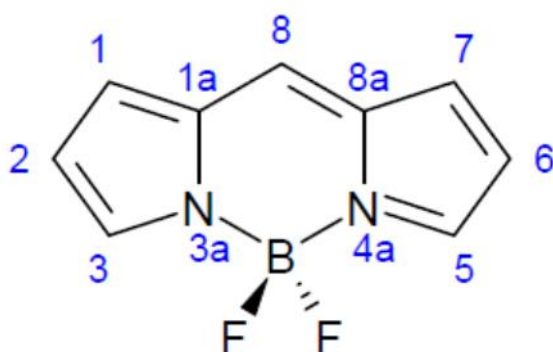
email: ines.corral@uam.es

ABSTRACT.

The potential tunability of the spectroscopic properties of the BODIPY parent dye by suitable functionalization makes it attractive for a number of applications. Unfortunately, its strong fluorescence against minor intersystem crossing to the triplet states prevents its application in photodynamic therapy. With the perspective of designing BODIPY derivatives with enhanced intersystem crossing, the goal of this work is two-fold: (i) investigate the main deactivation channels of the parent BODIPY following irradiation, paying particular attention to the accessibility of the triplet state potential energy surfaces, as well as the non-radiative pathways involving the second brightest more stable singlet electronic state, S_2 , and (ii) evaluate the performance of the computationally efficient second order algebraic-diagrammatic construction scheme for the polarization propagator, (ADC(2)) against the complete active space second-order perturbation theory (CASPT2) method. Three singlet/triplet crossings were found, all of them with small spin-orbit couplings, being the S_1/T_2 crossing the most plausible for the observed intersystem crossing yield. Methodologically, it is found that the ADC(2) method qualitatively reproduces the landscape of the potential energy profiles for the photophysical processes investigated; however, it systematically underestimates the energies of the stationary points and crossings of the same and different multiplicity, with the largest discrepancies found at S_1/S_0 crossing points. Our CASPT2 results provide a comprehensive picture of the landscape of the excited state potential energy surfaces of the parent BODIPY that might serve as a basis for the rational design of photosensitizers with a particular photophysical profile.

1. INTRODUCTION

BODIPY or boron-dipyrromethene dye (4,4-difluoro-4-bora-3a,4a-diaza-s-indacene), see Scheme 1, is probably one of the dyes with the widest application scope. The origin of its exquisite versatility relies on its endless possibilities of functionalization, which allow modulating its electronic structure and thus tuning its photophysical properties (absorption, emission maxima, fluorescence or triplet quantum yields) or optimizing its macromolecular chemical properties for a particular purpose (i.e. solubility, etc).



Scheme 1. Structure of the parent BODIPY with atom numbering.

For example, derivatization of the parent BODIPY with bulky hydrocarbon chains,^[1] such as acetoxypropyl or polymerizable methacryloyloxypropyl groups at positions 2 (and 6),^[2] see Scheme 1 for atom numbering, results in more efficient and photostable solid- and liquid-state lasers dyes compared to the parent compound or the reference dye PM567, substituted in 2 and 6 positions with ethyl groups. Introducing methyliodoacetamide groups in the BODIPY core has led to the synthesis of fluorophores that accomplish 3D mapping of proteins, through the monitoring of donor-donor energy migration.^[3] The ability to modulate BODIPYs' fluorescence upon functionalization has also been exploited for the design of efficient chemical sensors with applications in analytical, clinical or environmental sciences.^[4] Thus, the incorporation of an electron donor moiety along the BODIPY core is the basis of

BODIPY-based pH and cation sensors. In the case of pH sensors, the absorption of a photon triggers an electron transfer process between the substituent and the excited BODIPY core that quenches the fluorescence of the dye. At low pH values, however, BODIPY recovers its normal fluorescence, following the protonation of the electron donor group. As for the cation sensors, the donating group is usually incorporated in a size-selective macrocycle. The coordination of a cation to the macrocycle, in this case, decreases the redox potential of the electron-donating group allowing the recovery of the inherent photophysical properties of the dye. Following similar design principles, BODIPYs have been also utilized as antenna systems with attractive applications in the field of optoelectronics.^[5, 6] For instance, when electron donor substituents, either fully organic such as (2,4,5-trimethoxybenzene)^[7] or iminofullerene,^[8] or organometallic, such as ferrocene,^[9] are incorporated in the BODIPY core, relatively long-lived charge transfer states are generated, which are useful as photosynthetic antenna systems.

Another domain where functionalization of core BODIPY is of fundamental importance is the rational design of singlet oxygen photosensitizers for photodynamic therapy (PDT).^[10, 11] PDT^[12] is a clinical practice primarily focused on the treatment of certain types of cancer and pre-cancerous conditions, but lately also expanded to the cure of psoriasis, macular degeneration, diabetes or other infectious diseases.^[13-16] PDT exploits the interaction between a photosensitizer (PS), a source of light, and molecular oxygen.^[12] The success of PDT is based on its potential high selectivity: the PS is expected to preferentially accumulate in the target area, which is then locally irradiated with light of a particular wavelength.^[17, 18] Once the PS is electronically excited, its efficacy relies on the population of triplet states, which then interact with molecular oxygen or other substrates.^[19] According to the type of reaction undergone by the PS, two therapeutic mechanisms are known: when radical species are produced via

hydrogen abstraction or electron transfer between the PS and the substrate, the mechanism is referred to as Type I; when instead an energy transfer occurs between the PS and molecular oxygen, recovering the PS in its ground state, the mechanism is defined as Type II.^[20] Singlet oxygen, reactive oxygen species and radicals, generated both in Type I and Type II mechanisms, are the cytotoxic agents that cause cellular death by necrosis, autophagy or apoptosis.^[18] As Type II mechanism preserves the chemical form of the PS, it is preferred to Type I, allowing for more therapeutic cycles within a single administration.

Useful PSs for PDT need to fulfill a series of spectroscopic properties, such as (i) sharp absorption, preferably within the so-called therapeutic window (600-800 nm),^[17] and (ii) the efficient generation of triplet states carrying enough energy (1eV relative to the ground state) to produce $^1\text{O}_2$ from ground state $^3\text{O}_2$. Furthermore, properties such as (iii) high photo- and chemo-stability, (iv) solubility in both lipophilic and aqueous media, and (v) high light-dark toxicity ratios are also desirable.^[10, 11]

As for the spectroscopic properties, the high fluorescence quantum yield of the parent BODIPY dye, which amounts to $\phi_{\text{FL}}=90\pm5\%$,^[21] is considered a handicap for PDT, since emission represents, in fact, a competing process with intersystem crossing (ISC) to the triplet manifold.^[20] Indeed, a very low ISC quantum yield of 1.1% has been recorded for the core BODIPY.^[21] Moreover, its maximum of absorption is centered at $\lambda_{\text{max}} = 500 \text{ nm}$ and thus blue shifted with respect to the therapeutic window; therefore, efficient photoactivation of the dye, especially in deep tumors is not yet guaranteed.

These drawbacks, however, can be potentially circumvented taking advantage of its proneness to chemical functionalization,^[22] through which the photophysical properties could be adjusted. Several works in the literature have considered the introduction of heavy atoms to enhance singlet oxygen production in BODIPYs,^[23, 24] yet a balance

between high triplet quantum yields and acceptable light/dark toxicity ratio^[25, 26] or imaging and therapeutic combined effects,^[27] very useful at the first stages of in vivo/in vitro studies and further on in clinical trials has not been accomplished. In order to design BODIPYs showing an improved spectroscopic profile suitable for singlet oxygen photosensitization and fulfilling the additional clinical conditions, mentioned above, the dissection of the photophysics of the parent compound could provide a valuable basis to subsequently draw clear structure-photophysics relationships for different derivatives. As a first step towards the design of functionalized BODIPYs suitable for PDT, here, we revisit the deactivation mechanism of the parent BODIPY compound using state-of-the-art multiconfigurational methods, and compare the results with more economic single reference methods, such as coupled cluster and ab initio polarization propagator methods, which can afford the study of large BODIPY derivatives in the future. In particular, here we shall use CASPT2^[28] (second-order perturbation theory complete active space) and ADC(2).^[29]

Since the BODIPY core serves as a reference to monitor the effect of the different substitution patterns on the electronic transition,^[30, 31] its absorption spectrum is available for a wide range of computational protocols. However, only a few studies have transcended the Franck-Condon (FC) region and explored in detail the excited state potential energy surfaces (PES). Specifically, Briggs et al.^[32] characterized the S_1 excited state minimum and simulate the gas phase and water emission spectrum of BODIPY using an hybrid quantum mechanics/molecular mechanics (QM/MM) approach. The groups of Corminboeuf^[33] and Dede,^[34] additionally considered the non-radiative deactivation channel to the ground state thereby locating several S_1/S_0 conical intersections.

In this work, we focus on the specific role of the triplet states within the photophysics of the core BODIPY. We have explored the triplet PES and considered higher-lying singlet electronic excited states in order to investigate their participation in alternative internal conversion and intersystem crossing funnels to populate the triplet manifold. The present comprehensive description of the photophysics of BODIPY is expected to guide the design of new PS with an enhanced triplet quantum yield or with application in other domains where the irradiation energy is not subject to constraints.

COMPUTATIONAL DETAILS

The ground state geometry of the parent BODIPY was optimized with the B3LYP hybrid functional^[35] and the 6-311G** Pople basis set.^[36] This standard hybrid XC functional was chosen as it proved to predict geometries in good agreement with the experimental crystallographic structures and quite accurate vertical transition energies,^[37] according to the assessment performed by several density functional theory benchmark works on BODIPYs.^[38-40] Yet, its good behavior was ascribed to error cancellation, since in fact range-separated XC functional were found to be more suitable to qualitatively reproduce the experimental absorption spectra of BODIPYs.^[39, 41]

Since one of the goals of this work is to revisit the absorption spectrum of the parent BODIPY expanding the scope of methods used so far, the absorption spectrum was calculated in the framework of second order methods, including the algebraic diagrammatic construction scheme for the polarization propagator in its second-order scheme, ADC(2),^[29] and the single and doubles Coupled Cluster approximation, CC2.^[42] These calculations were performed in combination with the aug-cc-pVDZ^[43] basis and invoking the resolution of identity approximation^[44] to avoid four-index two electron integrals. The assessment of the performance of these methods, using the experimental absorption spectrum as a benchmark, will guide us in the selection of the

approach that represent a good compromise between accuracy and computational cost to reevaluate the deactivation mechanism of this system, which is the ultimate aim of this work. A better comparison with the experimental spectrum was achieved after convoluting the theoretical line spectra employing Lorentzian functions with half-widths of 13.5 nm.

Furthermore, the results were compared with those obtained with multistate-CASPT2 (MS-CASPT2).^[45] For the MS-CASPT2 calculation of the spectrum, we considered 5 roots, the standard IPEA shift^[46, 47] value of 0.25 a.u. and the 0.1 a.u. level shift value^[48] in conjunction with the large Atomic Natural Orbitals (ANO-L)^[49] basis set contracted to [3s2p/4s3p2d] for H and heavy elements, respectively. The active space (AS) comprises the complete set of π orbitals amounting to 12 active electrons in 11 orbitals (12,11), as recommended in Refs.^[30, 34] (see also **Figure S1 of the Supporting Information**). In passing, we also compare our results with those obtained using the protocol recommended by Jacquemin's group for BODIPYs,^[39-41] consisting of the time-dependent (TD) version of M06-2X^[50] exchange and correlation functional together with basis sets incorporating diffuse functions.

The most stable singlet excited state S_1 minimum was optimized with the TD-M06-2X/6-31+G(d,p),^[36] CC2/TZVP,^[42, 51] ADC(2)/TZVP and MS-CASPT2//CASSCF/6-31G* approaches. Other regions of the PES were explored with CASSCF/6-31G* and ADC(2)/TZVP protocols. The CASSCF/6-31G* stationary and degeneracy points of the PES were connected employing the Intrinsic Reaction Coordinate (IRC) method, following the Minimum Energy Path (MEP) of the excited state of interest.^[52] A total number of 3 roots were considered for the optimization of the excited states and conical intersections (CI), as well as for the MEP calculations. However, the final energies are

reported at MS(5)-CASPT2/CASSCF/ANO-L level of theory. The RICD approximation^[53] was used to compute two-electron integrals.

As inclusion of dynamical correlation was found to break the degeneracies located at the CASSCF level of theory at the position of the CI geometries, up to 1.0 eV, these geometries were refined following CASPT2 MEPs, based on SA(3)-CASSCF(12,11)/6-31G* wavefunctions. The CI geometries were considered converged when the energy difference between the two potential energy surfaces was roughly 0.13 eV, taking into account that radiationless jumps between two states do not necessarily occur at the vertex of the cone.^[54] Spin orbit coupling (SOC) at the S_1 minimum geometry and singlet/triplet crossing points have been estimated employing the relativistic Douglas-Kroll-Hess Hamiltonian^[55] and the Atomic Mean Field Integral approximation (AMFI).^[56] To calculate the SOC, we switched to the relativistic ANO-RCC basis set.^[57]

The calculations involving the S_1/S_0 -CI that present the N_{4a} -B bond broken (see below) required a slightly different active space in which the orbital HOMO-2, which at this point of the PES presents an occupancy of 1.99, is replaced for the lone pair localized on the N atom from the detached ring, with occupancy of 1.66 (see **Figure S3**).

The CASSCF and MS-CASPT2 calculations were performed employing the Molcas 7.8 software package.^[58] For the optimization of CASSCF conical intersections, we employed the Molpro 2009 package.^[59] TD-DFT calculations were carried out with the Gaussian 09 program^[60] while CC2 and ADC(2) methods were employed as implemented in Turbomole 6.5 package.^[61]

1. RESULTS AND DISCUSSION

2.1 Absorption spectrum

Figure 1a presents the gas phase multiconfigurational simulated absorption spectra of BODIPY core in the range between 2-6 eV together with the experimental absorption spectrum recorded in dichloromethane.^[21] The key band for PDT purposes is the one centered at 2.46 eV (503 nm),^[21] close to the “therapeutic window” (600-800 nm).^[12]

The CASPT2 method gives a good approximation to the first absorption band, only blue shifted by 0.18 eV. This deviation from the experimental result is ascribed to neglecting solvent dye interactions. Indeed, dichloromethane is expected to blue shift transitions which are less polar than the ground state, such as the S_1 ($\mu_{S0}=4.2819$ D vs. $\mu_{S1}=4.1037$ D). Our CASPT2 vertical excitation energy is slightly less accurate compared to the almost overlapping with the experimental energy value reported by Momeni and Brown,^[30] who employed the cc-pVTZ basis set.

The methods considered in Figure 1b, for the calculation of the absorption spectrum can be classified according to their deviation from the reference CASPT2 absorption spectrum, used as benchmark.

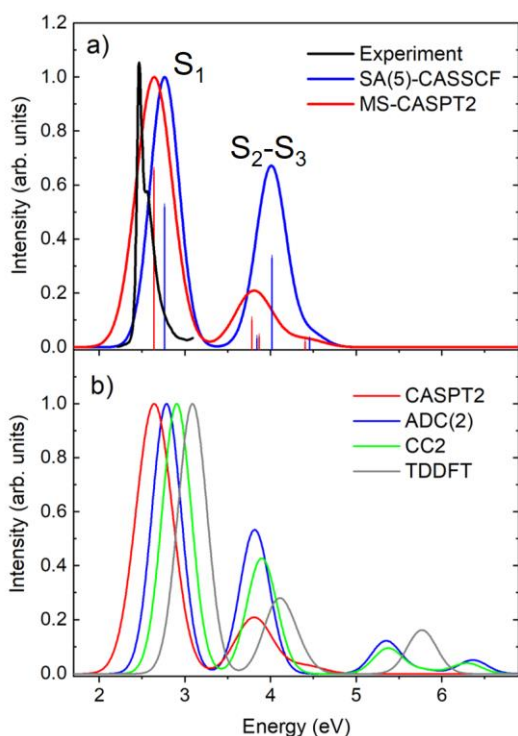


Figure 1. a) Simulated multiconfigurational and experimental^[21] absorption spectra of the parent BODIPY. Level of theory indicated in the legend. Line spectra indicating the transitions involved in each band are also included. b) Comparison of the performance of different monoconfigurational methods against the reference MS-CASPT2.

For the band peaking at 2.46 eV (500 nm), ADC(2) and CASSCF methods provide the smallest deviation amounting to 0.13 eV with respect to our CASPT2 reference. These deviations are ascribed to the lack of dynamic correlation of the CASSCF method, whilst ADC(2) suffers from neglecting static correlation and potential minor contributions of double excited states in the description of the wavefunction.^[62]

The CC2 absorption, in good agreement with the results reported by Petrushenko et al,^[31] provides a slightly worse result, deviating from CASPT2 by 0.26 eV.

TD-DFT delivers the largest deviation, of about 0.45 eV, compared to the CASPT2 value. This is ascribed to the inherent limitations of TD-DFT, which is known to have serious troubles in description of systems with multireference character and to account for the contribution of double excitations, which is the case of the BODIPY dye, as underlined by Momeni et al.^[30]

This first absorption band is mainly characterized as a HOMO-LUMO transition regardless of the employed method, see **Table 1**, albeit with significant differences in the weight of this configuration in the wave function, ranging from 50-95%, what might also explain the differences in the transition energies. Such a transition corresponds to a $\pi\pi^*$ excitation mainly localized on the pyrrole rings (**Figure S1**).

From the analysis of these results, we conclude that, at least for the description of the first absorption band, introducing static correlation seems to be as relevant as dynamic correlation.

Table 1. Characterization of the first absorption band of the parent BODIPY calculated at different levels of theory. Energy difference (ΔE in eV) relative to the experimental value is reported within parenthesis.

S₁ ($\pi\pi^*$)						
	ΔE (nm)	ΔE (eV)	f	Main Configuration		Weight (%)
TD-DFT	401.6	3.09 (0.63)	0.5	H	L	95.9
				H-1	L	3.6
CC2	427.2	2.90 (0.44)	0.5	H	L	83.7
				H-1	L	11.3
ADC(2)	445.4	2.78 (0.32)	0.51	H	L	84.2

				H-1	L	11.2
CASSCF	448.9	2.76 (0.3)	0.52	H	L	49.3
				H-1	L	21.8
CASPT2	469.7	2.64 (0.18)	0.65	H	L	63.7
				H-1	L	7.9

The clear trends observed for the energies of the first absorption band do not longer hold for the second and third electronic transitions, see [Figure 1](#) and [Table 2](#). In fact, if we consider the CASPT2 results as a reference, the second order CC2 and ADC(2) methods seem to outperform compared to CASSCF and TD-DFT, the latter providing the largest deviations. In contrast, a much larger discrepancy among all the methods is obtained regarding the intensity, with TD-DFT providing the best agreement with the CASPT2 results.

According to our calculations, the origin of the second band in the absorption spectrum of BODIPY, is the presence of two very close transitions, the S_2 and S_3 , see [Figure 1a](#) and [Table 2](#), with the S_2 contributing to a greater extent. The S_4 electronic state would be responsible for the shoulder at the blue side of this band. As in the S_1 , these $\pi\pi^*$ transitions, respectively involving the HOMO-1 and the LUMO and HOMO-2 and the LUMO orbitals, are strongly localized on the pyrrole heterocycles. Noticeably, whilst CASSCF and CASPT2 predict markedly multiconfigurational wavefunctions for the S_2 and S_3 states, the other methods employed predict contributions exceeding 90% from a single configuration.

Also worth noting is that the proximity of the S_2 and S_3 transitions leads to a different state ordering at the CASSCF and CASPT2 levels of theory. In fact, after incorporating

dynamical correlation, the S_3 HOMO-1 \rightarrow LUMO transition at CASSCF level stabilizes, becoming the S_2 , see [Table 2](#).

In summary, despite second order CC2 and ADC(2) miss important features of the electronic structure of the excited states of the parent BODIPY core at the FC region they do provide a good description of the absorption spectrum.

Table 2. Characterization of the second band of the parent BODIPY absorption spectrum with the different methods considered in our survey.

$S_2 (\pi\pi^*)$							$S_3 (\pi\pi^*)$					
	ΔE (nm)	ΔE (eV)	f	Main Configuration		Weight (%)	ΔE (nm)	ΔE (eV)	f	Main Configuration		Weight (%)
TD-DFT	304.3	4.07	0.12	H-1	L	95.7	289.4	4.28	0.04	H-2	L	98.4
				H	L	3.9						
CC2	319.6	3.88	0.19	H-1	L	82.8	309.7	4.00	0.04	H-2	L	92.3
				H	L	12.9				H-3	L	3.2
ADC(2)	326.3	3.80	0.24	H-1	L	83.7	316.7	3.92	0.04	H-2	L	92
				H	L	12				H-3	L	3.5
CASSCF	322.9	3.84	0.03	H-2	L	54.4	308.7	4.02	0.33	H-1	L	40.8
				(2) H-1/H ^a	L	16.6				H	L	20.8
										(2) H-2/H ^a	L	14.8
CASPT2	327.8	3.78	0.10	H-1	L	54.7	320.6	3.87	0.04	H-2	L	56.4
				H	L	6.4				(2) H-1/H ^a	L	17.7
				(2) H-2/H ^a	L	16						

^aDouble excitations.

2.2 Singlet Potential Energy Surfaces

Deactivation mechanism from the $S_1 \pi\pi^*$ electronic state

A comprehensive study of the photophysics of a dye requires the exploration of the excited and ground state PES beyond the FC region. To this purpose, we have undertaken MEP calculations following the gradients of the two lowest-lying electronic excited states, which are, according to all the methods investigated, ultimately responsible of the first two bands of the absorption spectrum.

The S_1 MEP connects, directly and only in few steps, the FC region with a minimum lying 2.63 eV above the ground state equilibrium structure, according to CASPT2. The energies for the S_1 minimum calculated with TD-DFT, CC2 and ADC(2) are 2.98 eV, 2.65 and 2.55 eV, respectively. In agreement with previous studies,^[30, 32] the structure of this stationary point differs from the ground state (See Table S1) in that it is no longer planar, neither symmetric. Also similarly to what was reported by Briggs et al.,^[32] TD-DFT predicts slightly smaller (B-N_{4a}-C_{8a}-C₈) dihedrals θ (recall Scheme 1 for atom numbering) compared to multiconfigurational approaches.

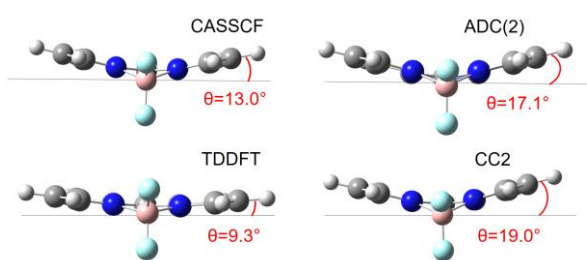


Figure 2. Side view of the S_1 minimum structures optimized with different methods. (B-N_{4a}-C_{8a}-C₈) dihedral angles θ (in degrees) for these methods are also indicated.

In fact, TD-M06-2X predicts a dihedral of 9.3° , that is, 4° smaller than CASSCF ($\theta = 13^\circ$), which predicts almost the same distortion from planarity than CASPT2 ($\theta = 14.4^\circ$)^[32]. Interestingly, ADC(2) calculates an intermediate dihedral of 17° , whilst the dihedral angle predicted by the CC2 method is the largest of all the methods considered and amounts to 19° .

The C_{2v} S_1 planar structures reported in previous works^[34] obtained by a geometry optimization initialized from planar initial guess structures or by imposing C_{2v} symmetry constraints along the optimization procedure, were found to correspond to transition states, in agreement with ref ^[32]. Indeed, the frequency calculation at TD-DFT level of theory presents an imaginary frequency of -17.5 cm^{-1} , which corresponds to the out of the plane oscillation of the B-F₂ moiety (see **Figure S2**) that, thus, connects the two equivalent non-planar S_1 minima.

Besides the deviation from planarity, the geometrical differences between the S_1 and the ground state equilibrium are rather small. At CASSCF level of theory, the main changes are localized in one of the two pyrrole rings for which the bond distances vary at most by $0.2\text{-}0.4\text{ \AA}$, whereas the largest decrease for the main angles is of 3.5° .

From the S_1 optimized structures, it is possible to calculate the vertical emission energies. As the relaxation energy of the S_1 state is minimal, the Stokes shift is very small. The experimental emission of the parent BODIPY was found to be influenced by the nature of the solvent and its maximum ranges from 2.42 eV ^[21] to 2.32 eV .^[63] Our gas phase CASPT2 simulations predict a value of 2.42 eV for vertical emission, while CC2 and ADC(2) calculate instead 2.48 eV and 2.32 eV , respectively. Our CASPT2 value is very close to that previously reported at 2.37 eV .^[32] Consistently with the predictions found for absorption, TD-DFT overestimates the emission energy by

delivering a value of 2.95 eV. Nevertheless, it should be noticed that TD-DFT emission energies are strongly functional depending, having been reported values comprised between 1.43 and 3.01 eV.^[30, 32]

The influence of the solvent on the emission spectrum can be ascribed to the change in the dipole moment of the S_0 and S_1 states compared to the FC region. Both states have, in fact, larger dipoles values at the S_1 minimum structure with respect to the FC geometry.

As the S_1/S_0 internal conversion funnel and its accessibility from the S_1 minimum are key features in the deactivation of photoexcited BODIPY core, they will be discussed in the following. The first S_1/S_0 -CI, showing a dissociated N-B bond, $(S_1/S_0)_{\text{dis}}$, was located 4.56 eV relative to the ground state equilibrium geometry and 1.93 eV above the S_1 minimum structure, at CASPT2 level of theory. At difference with the S_1 minimum, where CASSCF and CASPT2 approaches were found to provide very similar description of the PES, the region corresponding to the $(S_1/S_0)_{\text{dis}}$ funnel was found to be strongly sensitive to the addition of dynamic correlation, as well as to the number of roots considered in the calculation. Indeed, this degeneracy was uplifted by 0.65 eV upon inclusion of dynamic correlation to the reference CASSCF calculation.

This S_1/S_0 crossing smoothly connects with the minimum in the ground state, as depicted in **Figure S4a**. However, a geometry interpolation between the structures of the S_1 minimum and the S_1/S_0 conical intersection reveals the existence of an energetic barrier that would explain why it was not possible to leave the $(S_1/S_0)_{\text{dis}}$ seam of intersection while following the gradient of the S_1 state, see **Figure S4b**.

The CASPT2 geometry of the $(S_1/S_0)_{\text{dis}}$ -CI, reported in **Figure 3a**, involves a large structural reorganization with respect to the S_1 minimum. As already mentioned before,

accessing this funnel involves the rupture of the N_{4a}-B bond (recall Scheme 1 for atom numbering) and the rotation around the C₈-C_{8a} bond of the detached pyrrole ring that becomes almost orthogonal to the rest of the core structure. The dissociation of the B-N_{4a} bond triggers further rearrangements of the electronic and molecular structure of the system, which compromise its symmetry. For instance, the equivalent N_{3a}-B bond reinforces by 0.14 Å compared to the S₁ minimum structure, and the C_{1a}C₈C_{8a} bond angle centered on the *meso* carbon increases by 11°. These great structural modifications are at the origin of the energetic barrier showed in Figure S4.

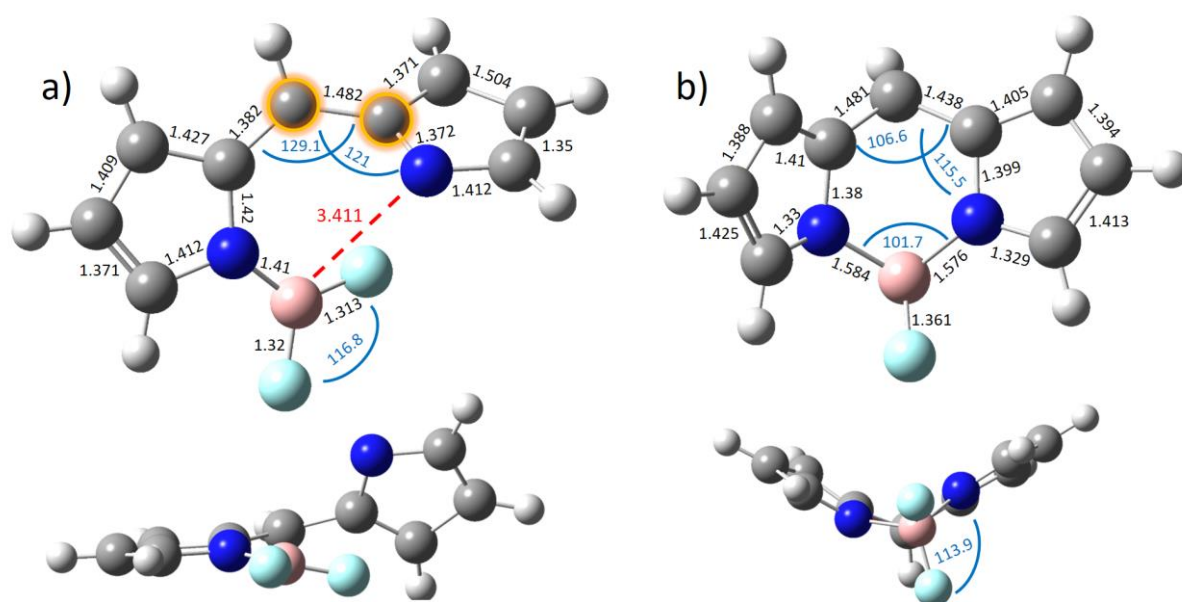


Figure 3. S₁/S₀-ClIs, (S₁/S₀)_{dis} (a) and (S₁/S₀)_{bent} (b), involving the FC S₁ electronic state, and resulting from exploring the PES with CASSCF and ADC(2) methods, respectively. Both structures were refined at the CASPT2//CASSCF level of theory. The figure includes front and side-views of the geometries and the main geometrical parameters. Bond lengths in Å and bond angles in degrees.

A similar S_1/S_0 -CI as the one described above was previously reported by Buyuktemiz et al.^[34] Nevertheless, there are important differences between these two funnels that affect both the energy and the structure, and thus deserve to be analyzed. The S_1/S_0 -CI reported in ref. ^[34] is located 3.1 eV relative to the minimum of the S_1 and 2.9 eV above the S_1 vertical excitation at the FC region, that is more than 1 eV above the equivalent crossing located in this work. Moreover, the geometry reported in ref. ^[34] is also slightly different than ours, as the CI reported by Buyuktemiz et al.^[34] exhibits a N_{4a} -B bond that weakens up to 1.981 Å, but that it is not yet broken. Our calculations confirm that the geometry reported by these authors is, indeed, a point of the CASSCF S_1/S_0 seam of intersection but the S_1/S_0 energy gap at CASPT2 level of theory is almost 1.3 eV.

For the sake of evaluating the validity of the ADC(2) method for the complete description of the PES of the parent BODIPY, we performed singlet point calculations at the geometry optimized with CASPT2. Interestingly and in line with previous observations that detect a systematic underestimation of the $\pi\pi^*$ state energies by ADC(2),^[62] we find that this method preserves the degeneracy between the S_1 and S_0 electronic states at the position of the $(S_1/S_0)_{\text{dis}}$ -CI, whilst predicts an energy of 3.85 eV, 0.7 eV below the value found at the CASPT2 level. The reliability of this calculation was assessed through the calculation of the D1 diagnostic, as implemented in Turbomole,^[64] which provides an estimate of the multireference character of the ground state wave function. The D1 value at this point of the PES amounted to 0.09, which is well over the tolerability limit for the use of monoconfigurational methods in the description of the ground state of a system. This is actually not surprising for a point of the PES where two electronic states are energetically degenerate and which presents a dissociated N-B bond.

Despite the non-rigorous characterization of S_1/S_0 -CIs made by the monoconfigurational ADC(2) method, its advantages to study the photophysics of medium to large systems are undeniable. Moreover, it has been demonstrated that even if ADC(2) is not able to properly describe the branching space of CIs, it is often able to predict reasonable geometries and energies for these points .^[33, 65, 66]

Consistently with the work of Corminboeuf et al,^[33] the optimization of the S_1/S_0 CI with the ADC(2) method led to a different CI located 2.85 eV over the ground state equilibrium minimum, and characterized by a butterfly-like folding of the pyrrole heterocycles along the C_8 -B axis, in the following addressed as $(S_1/S_0)_{\text{bent}}$, (see **Figure 3b**). A peculiar feature of this structure is the position of the H atom at the *meso* position. The C_8 -H bond has rotated and lies perpendicular to the plane of the molecule and almost parallel to one of the two B-F bonds. This $(S_1/S_0)_{\text{bent}}$ CI was also found to be a degeneracy point of the CASPT2 PES, with an energy of 3.52 eV. Thus, both in the CASPT2 and ADC(2) PESs the two S_1/S_0 -CIs would be separated by 1 eV energy difference, although these funnels are much more accessible (ca. 0.7 eV) in the ADC(2) PES.

Similarly to the $(S_1/S_0)_{\text{dis}}$ -CI, our MEP calculations for the bent-CI indicate that this structure is smoothly connected to S_0 minimum (**Figure S5**). In contrast to the dissociated-CI, however, the pathway connecting the $(S_1/S_0)_{\text{bent}}$ crossing with the S_1 minimum does not show any barrier. As for the S_1 minimum, the potential energy profile directly connecting the structure of the bent with the dissociated -CI is defined by the existence of an energy barrier, which reflects the important electron density reorganization that involves the breaking of the N_{4a} -B bond (see **Figure 4**).

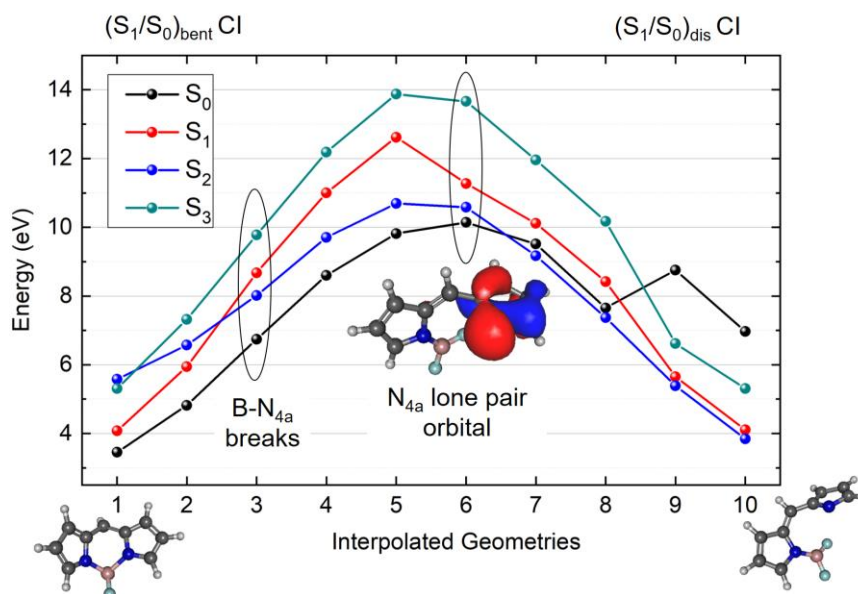


Figure 4. SA(5)-CASSCF(12,11)/6-31G* potential energy profiles along the linear interpolation in cartesian coordinates between $(S_1/S_0)_{\text{dis}}$ and $(S_1/S_0)_{\text{bent}}$ conical intersections.

Deactivation mechanism from the $S_2 \pi\pi^*$ electronic state

The reason for exploring the deactivation mechanism from higher lying excited states is twofold. On the one hand, there might be applications, other than PDT, where the use of high excitation energies to activate the photosensitizers is not a drawback; on the other hand, there are quite a few examples which reveal the importance of high lying excited states in the deactivation mechanism of systems even if they are not necessarily initially populated.^[67]

Our MEP from the FC region of the S_2 state very quickly reaches a degeneracy region between the two main spectroscopic states S_2/S_1 lying at 3.26 eV at the CASPT2 level of theory. The proximity between the FC region and the interstate crossing is reflected

in the similarity of the structure of the CI and that of the equilibrium ground state, as the molecule is still planar, with a (B-N_{4a}-C_{8a}-C₈) dihedral angle of only 0.5°. The initial C_{2v} symmetry is, however, lost with the B-N and C-C bonds asymmetrically modified around the axis defined by the C₈ and B atoms. The main geometrical parameters of the S₂/S₁-CI are reported in **Figure 5a**.

Consistently with the fact that no fluorescence has been observed from electronic states other than the S₁,^[21] the S₂/S₁ crossing is expected to represent an efficient internal conversion channel to transfer the S₂ population to the lower excited state.

The position of the ADC(2) S₂/S₁-CI slightly differs from the equivalent geometry calculated at the CASPT2 level of theory. At the position of the CASPT2 CI, the ADC(2) method predicts an energy gap of 0.24 eV and an energy value 0.13 eV below that predicted by CASPT2.

The ADC(2) S₂/S₁-CI is located 3 eV over the ground state equilibrium geometry, in agreement with the CASPT2 picture, and qualitatively reproduces the one obtained with the multiconfigurational CASPT2//CASSCF approach, considering that the largest deviations are of about 0.02 Å and 2° for bond distances and angles, respectively.

Within the CASPT2//CASSCF framework, a third non-radiative S_{1b}/S₀ channel was found at 5.36 eV, this time, the S₁ carrying the same character of the S₂ state at the FC region.

This S_{1b}/S₀-CI can funnel population from the second spectroscopic state back to the ground state, after the two spectroscopic states have crossed and the excited state order has changed, or alternatively from the S₁ spectroscopic state, assuming that the S_{1b}/S₀ crossing is energetically accessible from the S₁ minimum. The geometry of this degeneracy point, reported in **Figure 5b**, is twisted and deflects from the planar structure

characteristic of the previous S_2/S_1 -CI (Figure 5a). This deviation from planarity, however, is minor compared to that of the $(S_1/S_0)_{\text{bent}}$ -CI (Figure 3). The asymmetry of this CI also increases compared to the S_2/S_1 -CI. Major changes between these two CIs are localized on the B-N_{4a}, C_{8a}-N_{4a} and C₆-C₇ bond lengths that stretch by 0.139 Å, 0.11 Å and 0.138 Å, respectively, see Figure 5b.

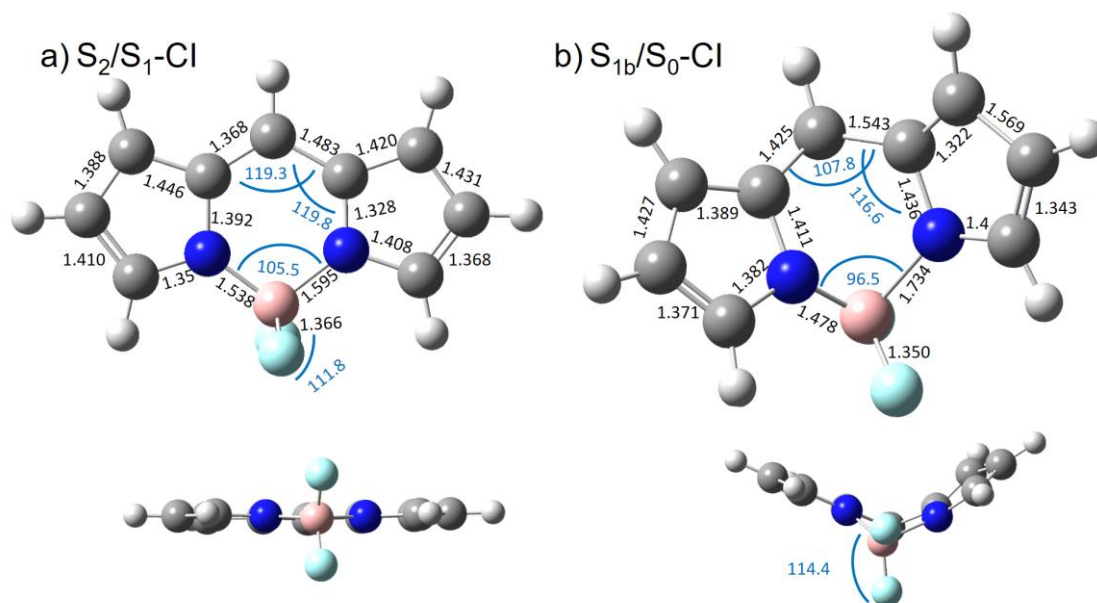


Figure 5. Side and front views of CASPT2 S_2/S_1 -CI (a) and S_{1b}/S_0 -CI (b) optimized geometries. Relevant bond distances in Å and angles in degrees are also reported.

Interestingly, our MEP calculations directly connect the S_{1b}/S_0 -CI with the S_1 minimum. Along the MEP, a smooth evolution of the S_1 character from the nature of the S_2 state at the FC region to that of the FC S_1 was observed. The smooth connection of the CI with the S_2/S_1 -CI was, however, not possible due to the presence of an energy barrier, see Figure S6.

The ADC(2) method also preserves the degeneracy of the CASPT2 S_{1b}/S_0 crossing, which lies 3.34 eV above the ground state minimum according to the second order

method. With a D1 value of 0.06, the trust limit value of this diagnostic is exceeded. Notably, the optimization of this point at the ADC(2) level results in the S_{1b} state degenerated with the S_0 at 3.8 eV. Coincidentally, at this point the FC S_1 lies very close in energy, which indicates that this geometry is better characterized as a three state degeneracy point.

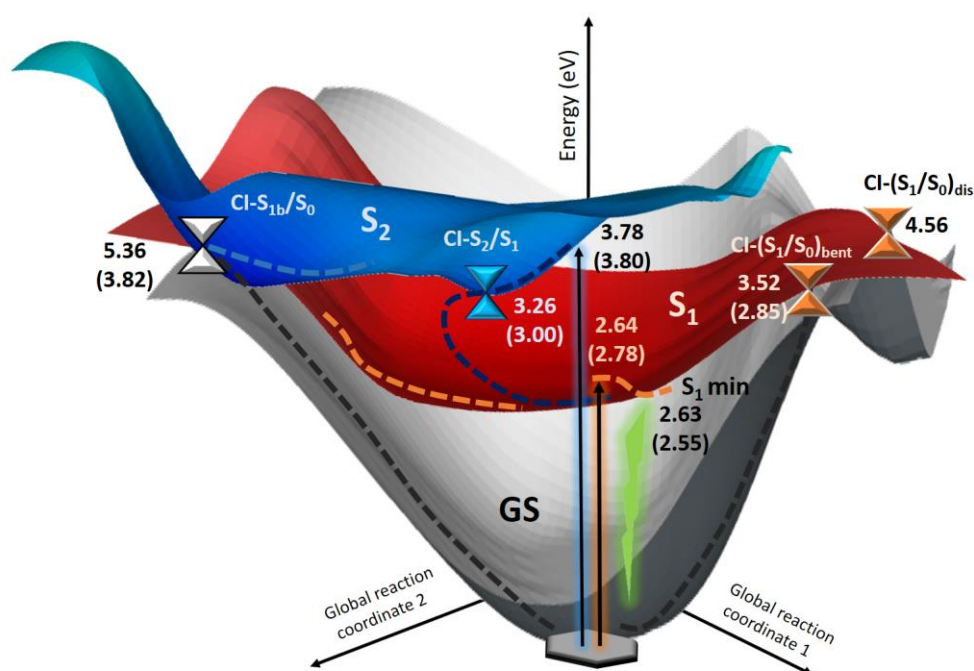


Figure 6. Schematic singlet state potential energy surfaces based on MEP calculations, minima and conical intersection (CI) optimizations. MS-CASPT2/ANO-L and ADC(2)/TZVP energies (in parenthesis) relative to the S_0 minimum in eV.

All in all, considering the landscape of singlet potential energy surfaces (see [Figure 6](#)), we can reasonably expect that the population reaching any of the two spectroscopic

states would be collected at the S_1 minimum. While the population of the S_2 state will relax via the S_2/S_1 internal conversion, nurturing the S_1 minimum, the population excited to S_1 will directly fall into this minimum.

As this minimum is separated from the S_1/S_0 -CIs by uphill potential energy profiles, emission seems to be the most reasonable relaxation route, in accordance to the large fluorescence quantum yield of $90\pm 5\%$ [21, 63] experimentally observed. Yet, ISC with a quantum yield of 1.1% has been also reported.[21] Thus, in the following, the role of the triplet states in the deactivation of this chromophore will be investigated.

2.3 Triplet Potential Energy Surfaces

Population of the triplet manifold from the S_1 state

With the purpose of investigating the minor deactivation pathway along the triplet manifold in the parent BODIPY chromophore, we have located potential ISC funnels along or in the proximity of the simulated singlet deactivation pathway. These features of the PES are key to PDT, since they serve as funnels for the population of triplet states that act as precursors of singlet oxygen and other reactive oxygen species, cytotoxic to cellular biomolecules.[10, 11] Singlet-triplet energy gaps and SOC values are the two key ingredients to qualitatively estimate the probability for ISC.[68]

As a first approach, we have calculated vertical triplet excitation energies at the equilibrium geometry, see Table 3. According to CASPT2, T_1 lies 0.7 eV below the brightest S_1 state, while T_2 and T_3 are 0.5 and 0.7 eV above it, respectively. The T_3 state also lies 0.5 eV below the S_2 . Besides the large energy gaps, since the three triplets share the same $\pi\pi^*$ character as the singlet spectroscopic states, the SOC is expected to be small, according to the El-Sayed rules.[69]

Table 3. Excitation energies (ΔE), singlet-triplet energy gaps (Δ_{S-T}) and characterization of the lowest-lying triplet excited states according to MS-CASPT2/ANO-L level of theory.

	ΔE (eV)	Δ_{S-T} (eV)		Main configuration		Weight (%)
T ₁	1.92	S ₁ 0.72		H	L	82
T ₂	3.11	S ₁ 0.47	S ₂ 0.67	H-1	L	71
T ₃	3.31	S ₁ 0.67	S ₂ 0.47	H-2	L	71

Since the S-T energy differences are still quite large at the FC region, and we presume that the population will directly evolve from the FC region towards the S₁ minimum structure, we performed vertical excitations along the MEP connecting these two points to monitor the singlet triplet energy differences. No singlet-triplet crossings, able to leak population to the triplet manifold before the population reaches the S₁ minimum, were found but at the S₁ minimum the S₁/T₁ energy gap decreases to 0.6 eV. Nevertheless, the T₂ is still the closest state lying 0.4 eV above the S₁.

The SOC values at the position of the S₁ minimum were computed to qualitatively estimate ISC probabilities at this point of the PES, where the wave packet is supposed to be retained for some time, before further decaying. As anticipated from the character of the singlet and the triplet wave functions involved, the calculated SOC values at this point are extremely small. For instance, the S₁ and T₂ coupling, which is the largest of the three closest triplet states, amounts to only 1 cm⁻¹. Such small SOC are common in certain BODIPYs, for instance amounting to 0.1 cm⁻¹ in isoindole- derivatives.^[70] Considering these poor SOC values and the large energy gaps (see above), other additional energetically accessible ISC points involving the S₁ state were sought.

A S_1/T_2 ISC point was found with CASPT2 2.85 eV above the ground state equilibrium geometry. At this point, the S/T energy difference is only of 0.1 eV and the calculated SOC amounts to 0.7 cm^{-1} . This S_1/T_2 ISC point lies very close both to the S_1 minimum and a minimum in the T_2 potential. Incidentally, the T_2 minimum coincides with a T_2/T_1 -CI. Thus, ISC via S_1/T_2 ISC point will eventually allow the transfer of the population to the lowest triplet state, with no further possibility to return to the singlet excited manifold.

Consistently with their energetic proximity, the S_1/T_2 ISC geometry (**Figure 7a**) is very close to the S_1 minimum structure, the main differences localized in the bond distances of one of the two pyrrole rings. These differences are, however, slightly larger when the comparison is made with the T_2 minimum structure. The S_1/T_2 ISC geometry is predicted to be more bent along the B-C₈ axis ($\theta=12^\circ$) compared to the T_2 minimum ($\theta=7.5^\circ$). Also noteworthy, for the T_2 minimum we register an important disruption of the initial C_{2v} geometry, the responsible being the BF₂ moiety which asymmetrically displaces towards one of the two pyrrole rings, leading to B-N bond distances which differ in ca. 0.2 \AA .

As already observed for other regions of the PES, the ADC(2) method slightly underestimates the energy of S_1/T_2 ISC point compared to CASPT2 (2.6 eV vs 2.8 eV). Thus, only minor differences are found between the geometries optimized for this crossing with these two methods, except for the dihedral angle, which, as observed for the S_1 minimum structure, (recall **Figure 2**), seem to be strongly dependent on the level of theory employed in the calculations. Thus, in the ADC(2) geometry the out-of-plane deviation for the S_1/T_2 ISC point was found to be 5° larger compared the CASSCF geometry. Also, differences in the bond distances of the heterocyclic scaffold calculated with these two methods were detected, but none of them was larger than 0.03 \AA .

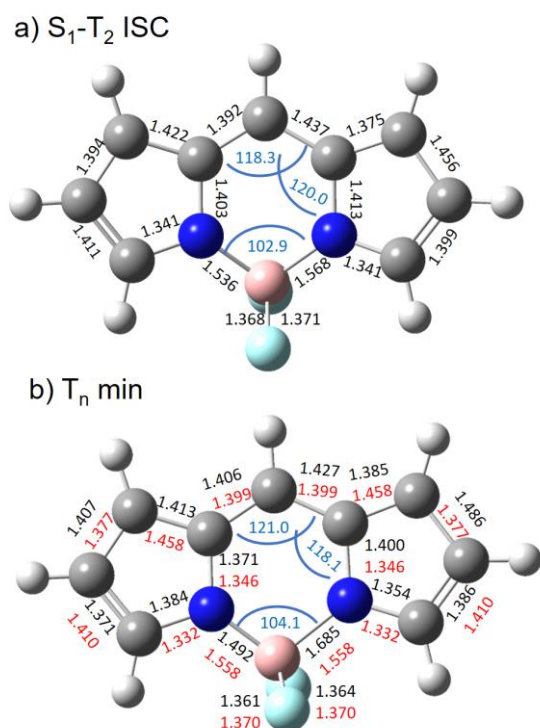


Figure 7. CASSCF S_1/T_2 ISC point (a) and T_1 and T_2 minimum (b) optimized geometries. Relevant bond lengths (in Å, red for T_1 and black for T_2) and angles (in degrees) are also presented.

Finally, a T_1 minimum structure was optimized and found to be planar and very similar to the ground state, as well as to the geometry reported by Buyuktemiz et al.^[34] At the CASPT2 level of theory, the T_1 minimum lies at 1.9 eV above the ground state minimum. Assuming its population is possible, the parent BODIPY could promote 1O_2 generation via an energy transfer process.^[20]

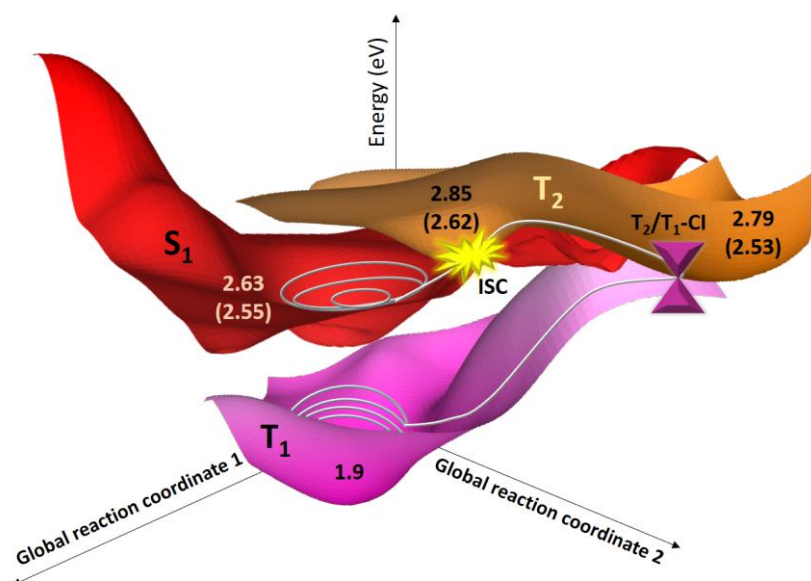


Figure 8. Schematic PESs including the lowest spectroscopic state S_1 , the closest triplet states T_1 and T_2 , and the position of the S_1/T_2 ISC and T_2/T_1 internal conversion funnels. The most probable pathway to populate the triplet manifold is highlighted. Relative energies in eV are reported for CASPT2 and ADC(2) in parenthesis.

To conclude, we have identified the most stable channel to transfer population from the lowest lying spectroscopic state S_1 to the triplet manifold, represented by the S_1/T_2 crossing point, see [Figure 8](#). The location of this point, close to the S_1 minimum structure, separated itself from S_1/S_0 funnels by high-energy barriers that would prevent the population from returning to the ground state, fulfills the energetic and structural requirements for an effective ISC, despite the very small values of the SOC. From the T_2 triplet state the molecule can subsequently relax via internal conversion to the T_1 , with enough energy to trigger the production of the cytotoxic 1O_2 employed in PDT.

Population of the triplet manifold from the S₂ state

Finally, as an alternative route to populate the triplet manifold, we have investigated deactivation from the S₂ state, even if this state is less relevant for PDT due to its higher absorption energy. According to CASPT2, at the FC region, the T₃ triplet excited state lies 0.5 eV below the S₂ but this difference could decrease as the S₂ state stabilizes. As a matter of fact, we have found an S₂/T₃ ISC point, lying 3.3 eV relative to the GS minimum, with a value for the SOC of 0.9 cm⁻¹. This value is still too small to make this ISC a competitive process but might be exploited for future BODIPY derivatives. Moreover, the S₂/T₃ ISC is expected to be strongly disfavored with respect to the S₂/S₁-CI for deactivation from the second spectroscopic state S₂. Interestingly, at the position of the S₂/T₃ ISC crossing, the S₁ and the T₂ states were also found to be energetically degenerate. This funnel is, however, higher in energy than the S₁/T₂ ISC crossing located along the deactivation of the S₁ state.

The ADC(2) method predicts an energy of 3.23 eV for the CASPT2 S₂/T₃ ISC crossing, while the optimization at the ADC(2) level results in an energy value for this crossing of 3.13 eV. At both geometries, the S₁ and T₂ states were found to be degenerate with ADC(2). From these results we can conclude that the ADC(2) and CASPT2 methods calculated very similar PESs, the ADC(2) energies being slightly more stable.

Finally, a last ISC funnel was found along the S₂ state. As it is located after the S₂/S₁ crossing, it actually corresponds to a S₁/T₁ crossing, where the S₁ has the character of the S₂ state at the FC region, similarly to what found at the S_{1b}/S₀-CI. At this point, with an energy of 3.16 eV and a SOC value of 1.24 cm⁻¹ we also find that the T₂ is energetically very close, leading to a three-degeneracy point. Following the same trend

as observed for the rest of the PES, the ADC(2) method confirms the S_{1b}/T_1 degeneracy at the position of the CASPT2 crossing at 2.77 eV, with T_2 in this case lying 0.3 eV above it. The optimization with ADC(2), instead, locates this crossing at 2.9 eV, with the T_2 state lying 0.4 eV higher in energy. This crossing would therefore compete with the S_2/S_1 internal conversion funnel.

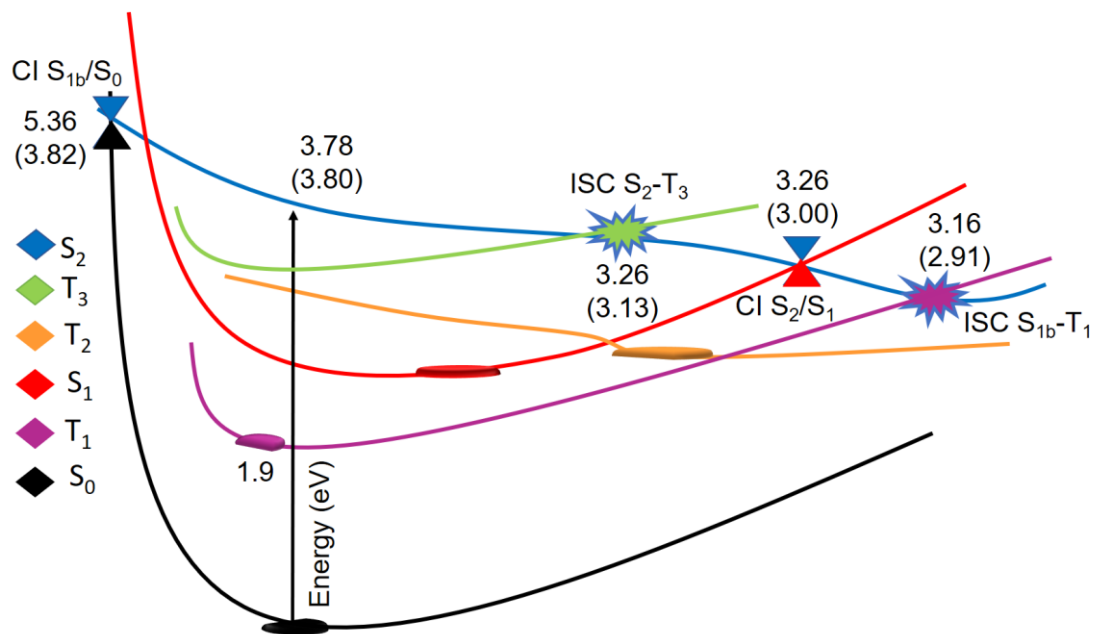


Figure 9. Schematic potential energy profile including the main stationary points, conical intersections (CI) and intersystem crossing (ISC) points from the S_2 spectroscopic state.

Conclusions

The deactivation mechanism of the parent BODIPY dye has been revisited using the ADC(2) and CASPT2 approaches. The topology of the ground and excited state potential energy surfaces has been investigated, paying special attention to the role of the triplets and higher-lying singlet excited states.

According to our CASPT2//CASSCF calculations, population directly excited to the S_1 state would evolve to a minimum in the same potential. Altogether, three different S_1/S_0 internal conversion crossings were located, differing both in the structure and character of the electronic states involved. The $(S_1/S_0)_{\text{dis}}$ crossing, previously reported by Buyuktemiz et al.,^[34] involves the dissociation of the B-N_{4a} bond. This funnel was located 1.93 eV above the S_1 minimum and 1.92 eV above the FC S_1 energy, but has been predicted to be 1.8 eV more stable than the equivalent crossing reported by these authors. The $(S_1/S_0)_{\text{bent}}$ crossing, previously reported by Prjl et al.,^[33] is characterized by a bent structure along the B-C₈ axis and is located 0.88 eV above the S_1 minimum. The S_{1b}/S_0 crossing is located beyond the S_2/S_1 conical intersection and thus involves an S_1 with the character of the FC S_2 . This structure was calculated 2.69 eV above the S_1 minimum. Taking the energy of the FC S_1 as a reference, none of these funnels would be accessible upon populating the S_1 . And interestingly, only the bent crossing, $(S_1/S_0)_{\text{bent}}$, would serve as a funnel for internal conversion to the ground state if the system is irradiated with wavelengths shorter than 300 nm, which corresponds to the center of the second absorption band.

Furthermore, three different singlet/triplet crossings were located along the minimum energy paths of the S_1 and S_2 states. Although energetically accessible, population transfer to the triplet manifold is not expected to be very efficient attending to the very small SOCs (0.7-1.25 cm⁻¹) calculated at these regions of the PES—in line with the very large fluorescence and very small triplet quantum yields experimentally observed.

Overall, the ADC(2) method was found to be able to qualitatively reproduce the landscape of the CASPT2 excited potential energy surfaces. However, several differences were found between the two methods. In general, the ADC(2) was found to underestimate the CASPT2 energies, except for the FC region where it provides slightly

higher vertical energies both for the S_1 and S_2 states, probably due to the overestimation of the monoconfigurational character of the wave functions by the ADC(2) method. Not unexpectedly, whilst the energetic deviation of ADC(2) from CASPT2 is rather small for excited state minima and interstate crossings, the discrepancies grow much larger for crossings involving the ground state, i.e. S_1/S_0 -CIs, (up to 1.5 eV), due to the incorrect description of the ground state made by the ADC(2), lacking static correlation, and the different description that this method makes of the ground and the excited states. Consistently, the D1 diagnostic at these points exceeds the tolerability limit for monoconfigurational protocols to reliably describe the ground state of this system. Nevertheless, at this point, it must be noted that $(S_1/S_0)_{\text{bent}}$ and $(S_1/S_0)_{\text{dis}}$ funnels would be accessible following excitation to the S_2 , but not upon excitation to the S_1 .

Finally, as for the geometries of the excited PES, ADC(2) method was also found to systematically overestimate the $(\text{B-N}_{4a}\text{-C}_{8a}\text{-C}_8)$ dihedral for bended structures, whilst coinciding with CASSCF in the remaining structural parameters.

In general, we have detected, from the analysis of the geometrical parameters for the different stationary point and interstates crossings, a correlation between the deviation from the planar structure of the BODIPY core and the increased asymmetry of the two fused pyrrole rings.

The present results should be useful towards the final goal of functionalizing the parent BODIPY for PDT so that internal conversion to the ground state is quenched, whilst SOC values are increased, in order to favor intersystem crossing to the triplet manifold. Non-adiabatic simulations could help to ponder the relevance of the different channels obtained in this work and thus unravelling other effects, which might help to enhance or suppress a particular channel. Work along these lines is in progress.

Acknowledgments

This work has been supported by the Project CTQ2015-63997- C2 of the Ministerio de Economía y Competitividad of Spain. I.C. gratefully acknowledges the “Ramón y Cajal” program of the Ministerio de Economía y Competitividad of Spain. M.D.V. thanks the Marie Curie Actions, within the Innovative Training Network-European Joint Doctorate in Theoretical Chemistry and Computational Modelling TCCM-ITN-EJD-642294, for financial support. L.G. thanks the University of Vienna. Computational time from the Centro de Computación Científica (CCC) of Universidad Autónoma de Madrid is also gratefully acknowledged.

References

- [1] K. K. Jagtap, D. K. Maity, A. K. Ray, K. Dasgupta and S. K. Ghosh, *Appl. Phys. B* 2011, **103**, 917-924.
- [2] F. J. Monsma, A. C. Barton, K. H. Choh, D. L. Brassard, R. P. Haugland and D. R. Sibley, *J. Neurochem.* 1989, **52**, 1641-1644.
- [3] F. Bergström, P. Hägglöf, J. Karolin, T. Ny and L. B.-Å. Johansson, *Proc. Nat. Acad. Sci.* 1999, **96**, 12477-12481.
- [4] U. Gilles, Z. Raymond and H. Anthony, *Angew. Chem. Int. Ed.* 2008, **47**, 1184-1201.
- [5] S. Debnath, S. Singh, A. Bedi, K. Krishnamoorthy and S. S. Zade, *J. Phys. Chem. C* 2015, **119**, 15859-15867.
- [6] H. Yeo, K. Tanaka and Y. Chujo, *Macromol.* 2013, **46**, 2599-2605.
- [7] S. Hattori, K. Ohkubo, Y. Urano, H. Sunahara, T. Nagano, Y. Wada, N. V. Tkachenko, H. Lemmetyinen and S. Fukuzumi, *J. Phys. Chem. B* 2005, **109**, 15368-15375.
- [8] A. Iagatti, L. Cupellini, G. Biagiotti, S. Caprasecca, S. Fedeli, A. Lapini, E. Ussano, S. Cicchi, P. Foggi, M. Marcaccio, B. Mennucci and M. Di Donato, *J. Phys. Chem. C* 2016, **120**, 16526-16536.
- [9] Y. V. Zatsikha, E. Maligaspe, A. A. Purchel, N. O. Didukh, Y. Wang, Y. P. Kovtun, D. A. Blank and V. N. Nemykin, *Inorg. Chem.* 2015, **54**, 7915-7928.
- [10] A. Kamkaew, S. H. Lim, H. B. Lee, L. V. Kiew, L. Y. Chung and K. Burgess, *Chem. Soc. Rev.* 2013, **42**, 77-88.
- [11] S. G. Awuah and Y. You, *RSC Adv.* 2012, **2**, 1169-11183
- [12] J. M. Dabrowski and L. G. Arnaut, *Photochem. Photobiol. Sci.* 2015, **14**, 1765-1780.
- [13] Y. K. Tandon, M. F. Yang and E. D. Baron, *Photoderm. Photoimmunol. Photomed.* 2008, **24**, 222-230.
- [14] R. P. L. Wormald, J. R. Evans, L. L. Smeeth and K. S. Henshaw, *Cochrane Database of Systematic Reviews* 2005, DOI: 10.1002/14651858.CD002030.pub2, CD002030.
- [15] J. P. Tardivo, F. Adami, J. A. Correa, M. A. S. Pinhal and M. S. Baptista, *Photodiag. Photodyn. Ther.* 2014, **11**, 342-350.
- [16] M. R. Hamblin and T. Hasan, *Photochem. Photobiol. Sci.* 2004, **3**, 436-450.
- [17] N. Mehraban and H. S. Freeman, *Materials (Basel)* 2015, **8**, 4421-4456.

- [18] I. O. Bacellar, T. M. Tsubone, C. Pavani and M. S. Baptista, *Int. J. Mol. Sci.* 2015, **16**, 20523-20559.
- [19] J. Zhao, K. Xu, W. Yang, Z. Wang and F. Zhong, *Chem. Soc. Rev.* 2015, **44**, 8904-8939.
- [20] M. C. DeRosa and R. J. Crutchley *Coord. Chem. Rev.* 2002, **233-234**, 351-371.
- [21] A. Schmitt, B. Hinkeldey, M. Wild and G. Jung, *J. Fluoresc.* 2009, **19**, 755-758.
- [22] A. Loudet and K. Burgess, *Chem. Rev.* 2007, **107**, 4891-4932.
- [23] R. Lincoln, A. M. Durantini, L. E. Greene, S. R. Martínez, R. Knox, M. C. Becerra and G. Cosa, *Photochem. Photobiol. Sci.* 2017, **16**, 178-184.
- [24] J. Zhao, K. Xu, W. Yang, Z. Wang and F. Zhong, *Chem. Soc. Rev.* 2015, **44**, 8904-8939.
- [25] N. Epelde-Elezcano, V. Martínez-Martínez, E. Peña-Cabrera, C. F. A. Gómez-Durán, I. L. Arbeloa and S. Lacombe, *RSC Adv.* 2016, **6**, 41991-41998.
- [26] J. H. Gibbs, Z. Zhou, D. Kessel, F. R. Fronczek, S. Pakhomova and M. G. H. Vicente, *J. Photochem. Photobiol. B: Biol.* 2015, **145**, 35-47.
- [27] M. J. Ortiz, A. R. Agarrabeitia, G. Duran-Sampedro, J. Bañuelos Prieto, T. A. Lopez, W. A. Massad, H. A. Montejano, N. A. García and I. Lopez Arbeloa, *Tetrahedron* 2012, **68**, 1153-1162.
- [28] K. Andersson, P. Å. Malmqvist and B. O. Roos, *J. Chem. Phys.* 1992, **96**, 1218-1226.
- [29] A. Dreuw and M. Wormit, *WIRE: Comput. Mol. Sci.* 2015, **5**, 82-95.
- [30] M. R. Momeni and A. Brown, *J. Chem. Theory Comput.* 2015, **11**, 2619-2632.
- [31] I. K. Petrushenko and K. B. Petrushenko, *Spectrochim. Acta A: Mol. Biomol. Spectrosc.* 2015, **138**, 623-627.
- [32] E. A. Briggs, N. A. Besley and D. Robinson, *J. Phys. Chem. A* 2013, **117**, 2644-2650.
- [33] A. Prlj, L. Vannay and C. Corminboeuf, *Helv. Chim. Acta* 2017, **100**, e1700093.
- [34] M. Buyuktemiz, S. Duman and Y. Dede, *J. Phys. Chem. A* 2013, **117**, 1665-1669.
- [35] A. D. Becke, *J. Chem. Phys.* 1993, **98**, 1372-1377.
- [36] R. Ditchfield, W. J. Hehre and J. A. Pople, *J. Chem. Phys.* 1971, **54**, 724-728.
- [37] G. Mazzone, A. D. Quartarolo and N. Russo, *Dyes and Pigments* 2016, **130**, 9-15.
- [38] C. Adamo and D. Jacquemin, *Chem. Soc. Rev.* 2013, **42**, 845-856.
- [39] D. Jacquemin, A. Planchat, C. Adamo and B. Mennucci, *J. Chem. Theory Comput.* 2012, **8**, 2359-2372.
- [40] B. Le Guennic and D. Jacquemin, *Acc. Chem. Res.* 2015, **48**, 530-537.
- [41] S. Chibani, B. Le Guennic, A. Charaf-Eddin, A. D. Laurent and D. Jacquemin, *Chem. Sci.* 2013, **4**, 1950-1963.
- [42] O. Christiansen, H. Koch and P. Jørgensen, *Chem. Phys. Lett.* 1995, **243**, 409-418.
- [43] D. E. Woon and J. T. H. Dunning, *J. Chem. Phys.* 1993, 1358-1371.
- [44] C. Hättig and F. Weigend, *J. Chem. Phys.* 2000, **113**.
- [45] J. Finley, P.-Å. Malmqvist, B. O. Roos and L. Serrano-Andrés, *Chem. Phys. Lett.* 1998, **288**, 299-306.
- [46] G. Ghigo, B. O. Roos and P.-Å. Malmqvist, *Chem. Phys. Lett.* 2004, **396**, 142-149.
- [47] J. P. Zobel, J. J. Nogueira and L. González, *Chem. Sci.* 2017, **8**, 1482-1499.
- [48] B. O. Roos and K. Andersson, *Chem. Phys. Lett.* 1995 **245**, 215-223.
- [49] K. Pierloot, B. Dumez, P.-O. Widmark and B. O. Roos, *Theor. Chim. Acta* 1995, 87-114.
- [50] Y. Zhao and D. G. Truhlar, *Theor. Chem. Acc.* 2007, **120**, 215-241.
- [51] K. E. Yousaf and K. A. Peterson, *J. Chem. Phys.* 2008, **129**, 184108.
- [52] P. Celani, M. A. Robb, M. Garavelli, F. Bemardi and M. Olivucci, *Chem. Phys. Lett.* 1995, **243**, 1-8.
- [53] F. Aquilante, R. Lindh and T. B. Pedersen, *J. Chem. Phys.* 2007, 114107-114107.
- [54] T. J. Martínez and S. Yang, in *Advanced Series in Physical Chemistry: Conical Intersections*, 2011, pp. 347-374.
- [55] M. Reiher, *Theor. Chem. Acc.* 2006, **116**, 241-252.
- [56] B. A. Heß, C. M. Marian, U. Wahlgren and O. Gropen, *Chem. Phys. Lett.* 1996, **251**, 365-371.

- [57] B. O. Roos, R. Lindh, P. Å. Malmqvist, V. Veryazov and P.-O. Widmark, *J. Phys. Chem. A* 2004, **108**, 2851-2858.
- [58] F. Aquilante, L. De Vico, N. Ferré, G. Ghigo, P. Å. Malmqvist, P. Neogrády, T. B. Pedersen, M. Pitonak, M. Reiher, B. O. Roos, L. Serrano-Andrés, M. Urban, V. Veryazov and R. Lindh, *J. Comput. Chem.* 2010, **31**, 224-224.
- [59] H.-J. Werner, P. J. Knowles, G. Knizia, F. R. Manby and M. Schütz, *WIRE: Comput. Mol. Sci.* 2012, **2**, 242-253.
- [60] M. J. Frisch, G. W. Trucks, H. B. Schlegel, G. E. Scuseria, M. A. Robb, J. R. Cheeseman, G. Scalmani, V. Barone, B. Mennucci, G. A. Petersson, H. Nakatsuji, M. Caricato, X. Li, H. P. Hratchian, A. F. Izmaylov, J. Bloino, G. Zheng, J. L. Sonnenberg, M. Hada, M. Ehara, K. Toyota, R. Fukuda, J. Hasegawa, M. Ishida, T. Nakajima, Y. Honda, O. Kitao, H. Nakai, T. Vreven, J. A. Montgomery, J. E. Peralta, F. Ogliaro, M. Bearpark, J. J. Heyd, E. Brothers, K. N. Kudin, V. N. Staroverov, R. Kobayashi, J. Normand, K. Raghavachari, A. Rendell, J. C. Burant, S. S. Iyengar, J. Tomasi, M. Cossi, N. Rega, J. M. Millam, M. Klene, J. E. Knox, J. B. Cross, V. Bakken, C. Adamo, J. Jaramillo, R. Gomperts, R. E. Stratmann, O. Yazyev, A. J. Austin, R. Cammi, C. Pomelli, J. W. Ochterski, R. L. Martin, K. Morokuma, V. G. Zakrzewski, G. A. Voth, P. Salvador, J. J. Dannenberg, S. Dapprich, A. D. Daniels, Farkas, J. B. Foresman, J. V. Ortiz, J. Cioslowski and D. J. Fox, *Gaussian 09, Revision B.01*, Wallingford CT, 2009.
- [61] F. Furche, R. Ahlrichs, C. Hättig, W. Klopper, M. Sierka and F. Weigend, *WIRE: Comput. Mol. Sci.* 2014, **4**, 91-100.
- [62] S. Knippenberg, M. V. Bohnwagner, P. H. Harbach and A. Dreuw, *J. Phys. Chem. A* 2015, **119**, 1323-1331.
- [63] I. J. Arroyo, R. Hu, G. Merino, B. Z. Tang and E. Pena-Cabrera, *J. Org. Chem.* 2009, **74**, 5719-5722.
- [64] C. L. Janssen and I. M. B. Nielsen, *Chem. Phys. Lett.* 1998, **290**, 423-430.
- [65] A. Prlj, A. Fabrizio and C. Corminboeuf, *Phys. Chem. Chem. Phys.* 2016, **18**, 32668-32672.
- [66] D. Tuna, D. Lefrancois, L. Wolanski, S. Gozem, I. Schapiro, T. Andruniow, A. Dreuw and M. Olivucci, *J. Chem. Theory Comput.* 2015, **11**, 5758-5781.
- [67] L. Martínez-Fernández, I. Corral, G. Granucci and M. Persico, *Chem. Sci.* 2014, **5**, 1336-1347.
- [68] C. M. Marian, *WIRE: Comput. Mol. Sci.* 2012, **2**, 187-203.
- [69] M. A. El-Sayed, *J. Chem. Phys.* 1963, **38**, 2834-2838.
- [70] M. E. Alberto, B. C. De Simone, G. Mazzone, A. D. Quartarolo and N. Russo, *J. Chem. Theory Comput.* 2014, **10**, 4006-4013.